

Wind-forcing comparison in INALT20

Authors: Kristin Burmeister, Franziska Schwarzkopf, Arne Biastoch, Peter Brandt, Joke Luebbecke, Mark Inall

Aim:

In this study the difference between the COREv2 (Griffies et al. (2009)) and JRA55-do (Tsujino et al. (2018)) forcing in INALT20 (Schwarzkopf et al. (2019)) is investigated with respect to the upper wind-driven ocean circulation in the tropical Atlantic. Where possible, the model outputs are validated and the analysis is extended by observational data.

Motivation:

The COREv2 wind forcing is known to exhibit spurious multidecadal wind variability (Hurrell and Trenberth, 1998; Fiorino, 2000; He et al., 2016). This presumably impacts the multidecadal variability of the wind-driven circulation in the tropical Atlantic in model simulation forced by COREv2. The upper wind-driven circulation in the tropical Atlantic plays a key role in the basin wide distribution of water mass properties and affects the transport of heat, salt and biogeochemical components like oxygen (Fig. 1 and e.g. Schott, McCreary Jr., and Johnson (2004), Hazeleger and Drijfhout (2006), Oschlies et al. (2018)). It is an important feature of the Atlantic climate system and the marine ecology in a warming world. Hence, it is crucial to improve the understanding of its long-term variability which is largely depending on model simulation due to sparse observational data coverage in earlier periods.

With INALT20 we have the opportunity to compare COREv2 with the new JRA55-do forcing, identify differences in both forcings and learn more about the multidecadal variability of the tropical Atlantic.

Comparison between JRA55-do and COREv2 in INALT20

As first step I calculated relative wind stress anomalies with respect to the 1958-2009 seasonal cycle based on monthly mean data of the host model ($1/4^\circ$). Then I calculate the annual mean of the anomalies and spatially average them between 3°S and 3°N for 10° -wide zonal boxes along the equatorial Atlantic (Fig. 2 and 3). Please note, similar results are obtained using the nested model ($1/20^\circ$) (see `1_INALT_JRA_CORE_taux_anomaly_3s3n_40w10e.png` and `1_INALT_JRA_minus_CORE_taux_anomaly_3s3n_40w10e.png` in the GitHub repository).

The difference in zonal wind stress anomalies increase to the east of the basin (Fig. 2 and 3).

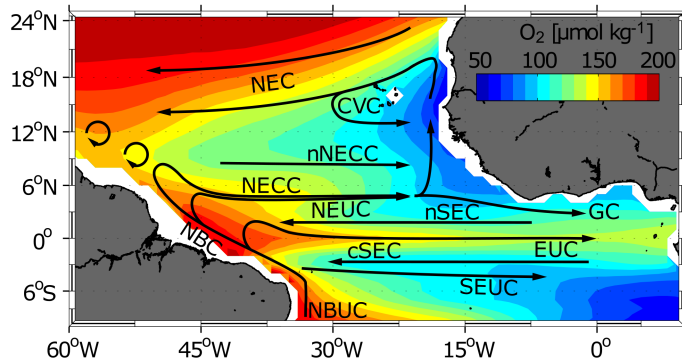


Figure 1: Oxygen concentration in $\mu\text{mol kg}^{-1}$ (shaded colors) averaged between 100 m and 200m depth obtained from MIMOC (Schmidtko, Stramma, and Visbeck (2017)). Superimposed are surface and thermocline (about upper 300 m) currents (black solid arrows; adapted from Hahn et al. (2017)): the North Equatorial Current (NEC), Cape Verde Current (CVC), North Equatorial Counter-current (NECC), northern branch of the NECC (nNECC), North Equatorial Undercurrent (NEUC), Guinea Current (GC), northern and central branches of the South Equatorial Current (nSEC, cSEC), Equatorial Undercurrent (EUC), South Equatorial Undercurrent (SEUC), North Brazil Current (NBC) and North Brazil Undercurrent (NBUC). This figure is adapted from K. Burmeister et al. (2019).

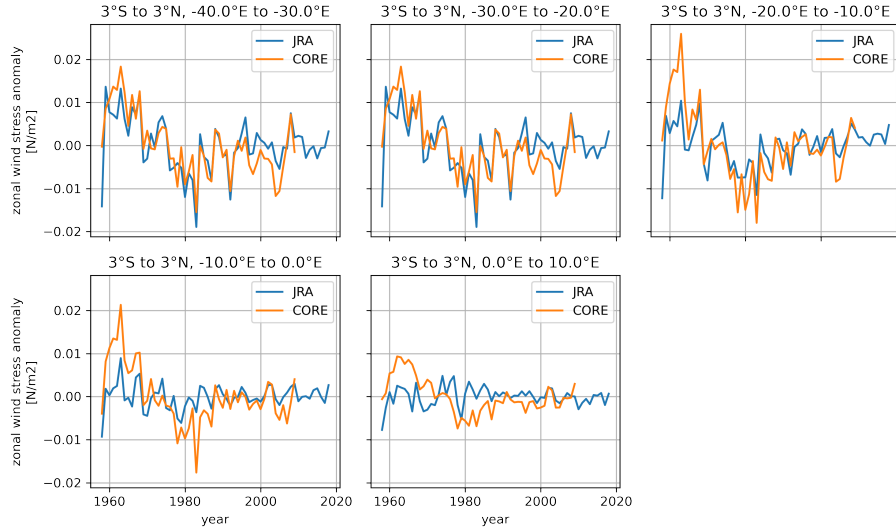


Figure 2: Annual mean wind stress anomalies with respect to the 1958-2009 climatology spatially averaged between 3°S and 3°N for 10° -wide zonal boxes along the equatorial Atlantic.

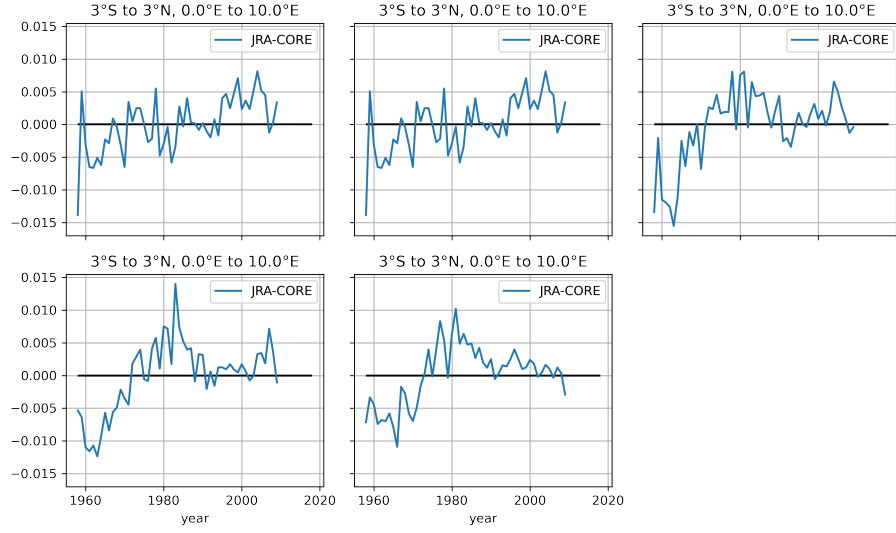


Figure 3: Difference of annual mean wind stress anomalies between JRA and CORE forcing (see Fig. 2).

But only for the period before 1990 - afterwards they agree quite well in the easter basin, whereas, at approximately the same time (late 1990s), they begin to deviate from each other in the western boxes.

For a better presentation of the difference of the forcings depending on the longitude I created hovmoeller diagrams of zonal wind stress anomalies latidunal averaged for diffrent longitudinal bands (Fig. 4 to 8).

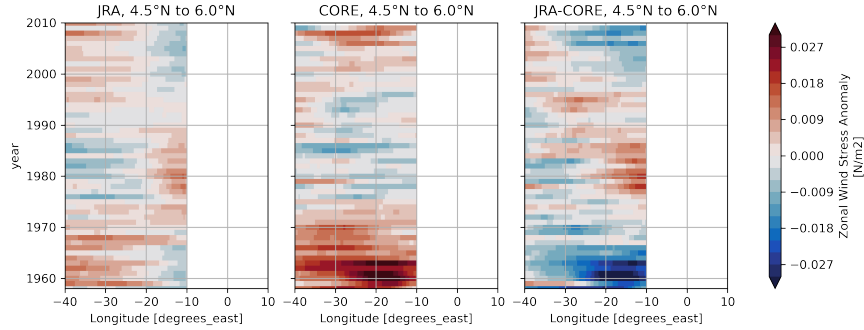


Figure 4: Hovmoeller diagram of annual mean wind stress anomalies with respect to the 1958-2009 climatology latitudinally averaged between 4.5°N and 6°N in the tropical Atlantic. The left panel shows wind stress anomalies of JRA, the middle one of CORE, and the right one of JRA minus CORE.

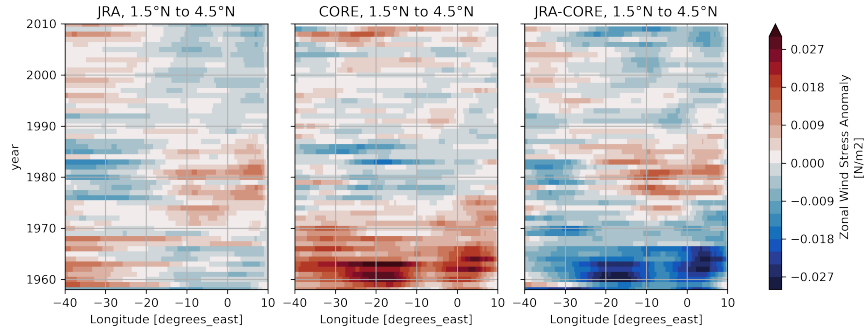


Figure 5: Hovmoeller diagram of annual mean wind stress anomalies with respect to the 1958-2009 climatology latitudinally averaged between 1.5°N and 4.5°N in the tropical Atlantic. The left panel shows wind stress anomalies of JRA, the middle one of CORE, and the right one of JRA minus CORE.

In general, the CORE zonal wind stress anomalies in the CORE forcing are stronger and zonally coherent (Fig. 4 to 8 centre). In JRA, north of the equator, zonal wind anomalies are not zonally coherent and reverse sign at about 20°W (Fig. 4 to 8 left). Differences between JRA and CORE increases from south to

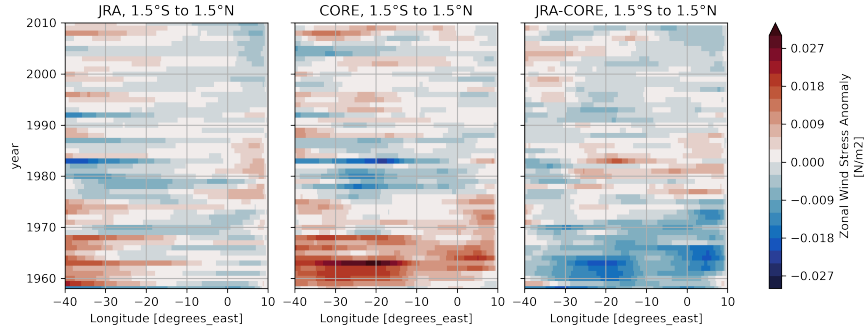


Figure 6: Hovmoeller diagram of annual mean wind stress anomalies with respect to the 1958-2009 climatology latitudinally averaged between 1.5°S and 1.5°N in the tropical Atlantic. The left panel shows wind stress anomalies of JRA, the middle one of CORE, and the right one of JRA minus CORE.

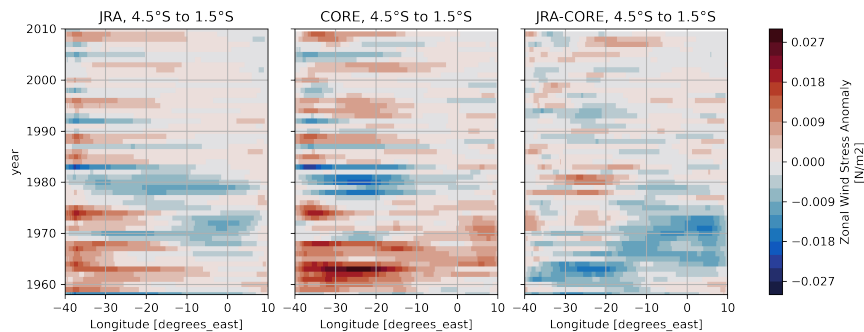


Figure 7: Hovmoeller diagram of annual mean wind stress anomalies with respect to the 1958-2009 climatology latitudinally averaged between 4.5°S and 1.5°S in the tropical Atlantic. The left panel shows wind stress anomalies of JRA, the middle one of CORE, and the right one of JRA minus CORE.

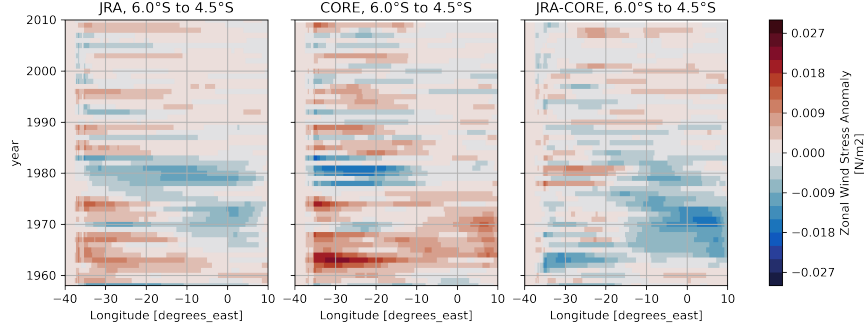


Figure 8: Hovmoeller diagram of annual mean wind stress anomalies with respect to the 1958–2009 climatology latitudinally averaged between 6°S and 4.5°S in the tropical Atlantic. The left panel shows wind stress anomalies of JRA, the middle one of CORE, and the right one of JRA minus CORE.

north (Fig. 4 to 8 right). This is also clearly visible in the meridional section of zonal wind stress anomalies along 23°W (Fig. 10).

The largest differences (up to $\pm 0.03 \text{ N m}^{-2}$) between both forcings occur east of 30°W before 1990 (Fig. ??). With CORE showing stronger eastward wind stress anomalies compared to JRA between 1958 and 1970 and stronger westward wind stress anomalies between 1970 and 1990.

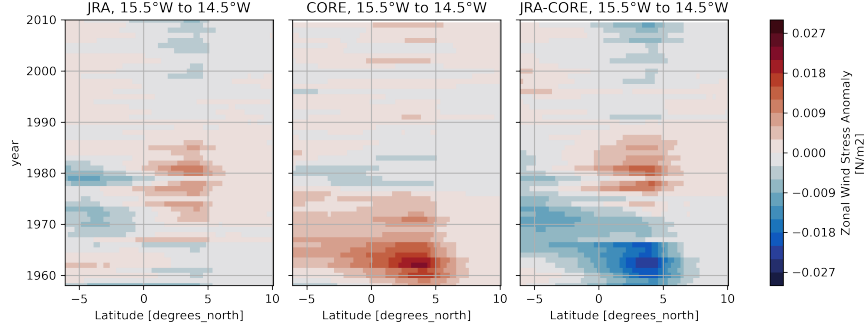


Figure 9: Hovmoeller diagram of annual mean wind stress anomalies with respect to the 1958–2009 climatology longitudinally averaged between 15.5°W and 14.5°W in the tropical Atlantic. The left panel shows wind stress anomalies of JRA, the middle one of CORE, and the right one of JRA minus CORE.

Zonal velocity along 23°W : INATL20 and observation

To validate INALT20 we compare it to longterm observations along 23°W . Currently an updated version of a mean section along 23°W is work in progress.

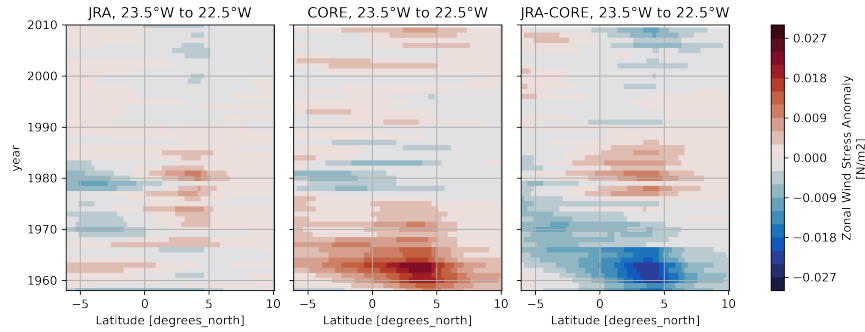


Figure 10: Hovmoeller diagram of annual mean wind stress anomalies with respect to the 1958–2009 climatology longitudinally averaged between 23.5°W and 22.5°W in the tropical Atlantic. The left panel shows wind stress anomalies of JRA, the middle one of CORE, and the right one of JRA minus CORE.

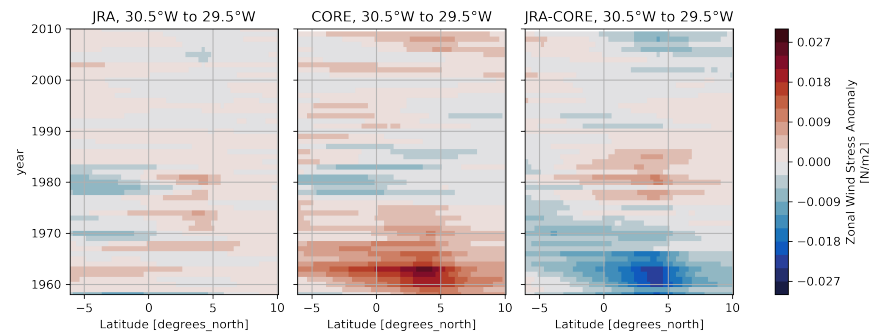


Figure 11: Hovmoeller diagram of annual mean wind stress anomalies with respect to the 1958–2009 climatology longitudinally averaged between 30.5°W and 29.5°W in the tropical Atlantic. The left panel shows wind stress anomalies of JRA, the middle one of CORE, and the right one of JRA minus CORE.

For now I compare the model to published mean section along 23°W (Brandt et al. (2015), Kristin Burmeister et al. (2020)). Lets start with the comparison of the simulated zonal velocities along 23°W of the JRA and CORE forcings (Fig. 12).

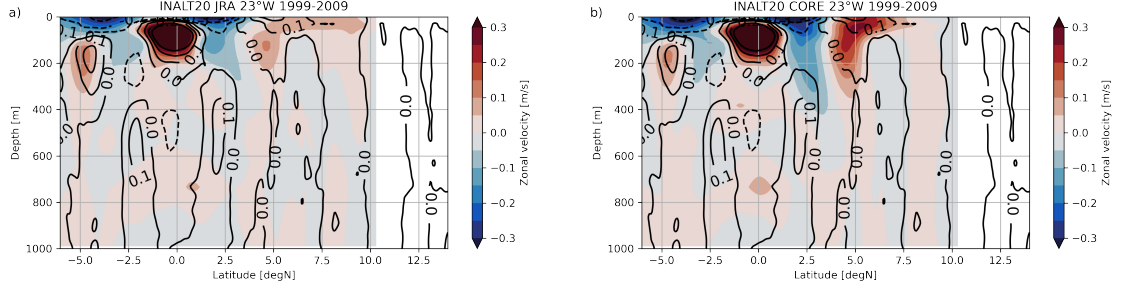


Figure 12: Zonal velocities along 23°W from INALT20 forced by a) JRA and b) CORE averaged for the period 1999-2009 (shading). Black contours mark observed zonal velocities averaged for the 1999-2012 period (Brandt et al., 2015).

The westward flowing nSEC (centered at about 2.5°N) and the eastward flowing NEUC (centered at about 5°N) are stronger and extend further down (~ 200 m for JRA, 400m for CORE) in the simulation forced by CORE (Fig. 12). Overall, JRA forced zonal velocities seems to be closer to observation (Fig. 12, 13 and 14) as the CORE forced ones. However, the nNECC (centered about 8.5°N) seemed to be better simulated by the CORE forcing (Fig. ??). Please note that the northern boundary of the nest is 10°N and the nNECC is located close to it.

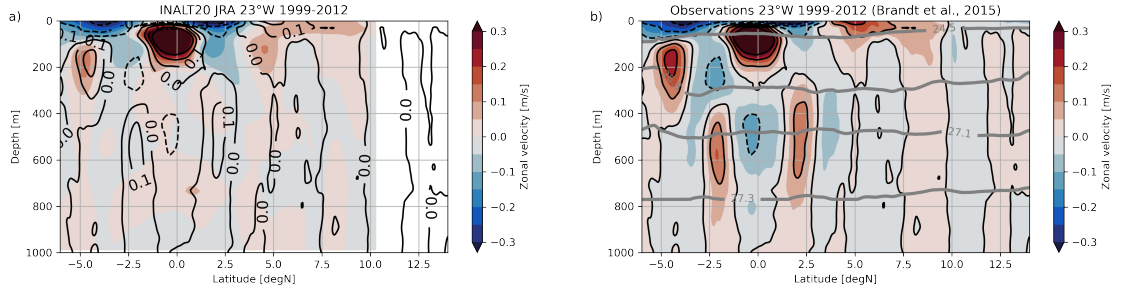


Figure 13: a) INALT20 and b) observed (Brandt et al., 2015) zonal velocity section along 23°W averaged for the period 1999-2012 (shading). Black contours mark observed zonal velocities, grey contours in b) mark potential density in kg m^{-3} .

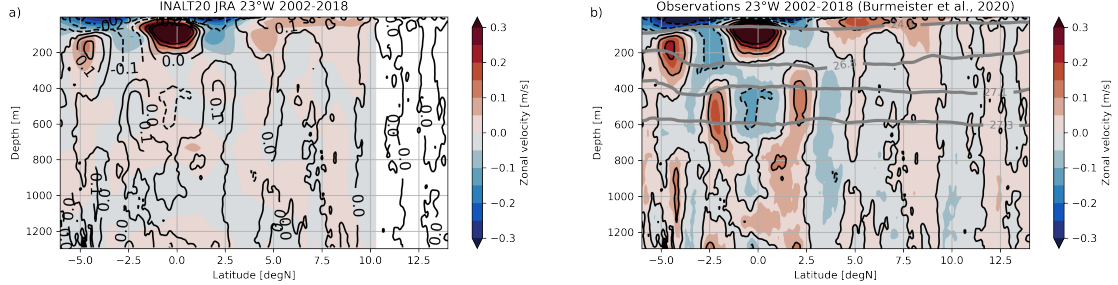


Figure 14: a) INALT20 and b) observed (Burmeister et al., 2020) zonal velocity section along 23°W averaged for the period 2002-2018 (shading). Black contours mark observed zonal velocities, grey contours in b) mark potential density in kg m^{-3} .

EUC transport at 23°W

To get a first impression, I calculated the EUC transport along 23°W after Brandt et al. (2014), i.e. only positive (eastward) velocities are integrated between 1.2°S and 1.2°N , 30m and 300m. I did that as a first step to compare the results to Brandt et al. (2014) (Fig. 16). The used observational dataset is from Kristin Burmeister et al. (2020) (7 cruises during 2006-2012) and apparently not all cruises from Brandt et al. (2014) (12 cruises during 2006-2012) are included. Unfortunately until now I could not find a list of the cruises used in Brandt et al. (2014) but all cruises should be included in the updated 23°W which is currently work in progress. Next, I will use the algorithm of Hsin and Qiu (2012) to calculate current transports, their central latitude and core depth.

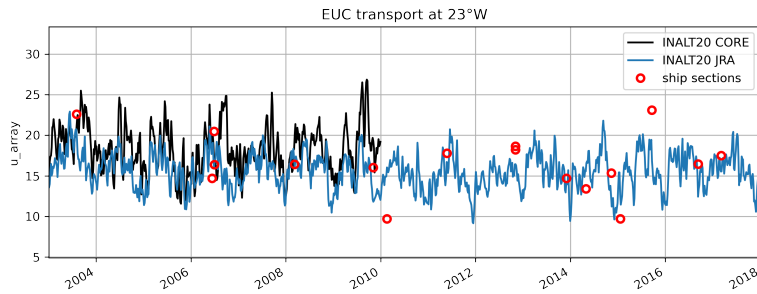


Figure 15: EUC transports at 23°W calculated from INALT20 model output (blue line for JRA, black line for CORE) and shipboard zonal velocities (red circles). For the transport only positive (eastward) velocities are integrated between 1.2°S and 1.2°N , 30m and 300m.

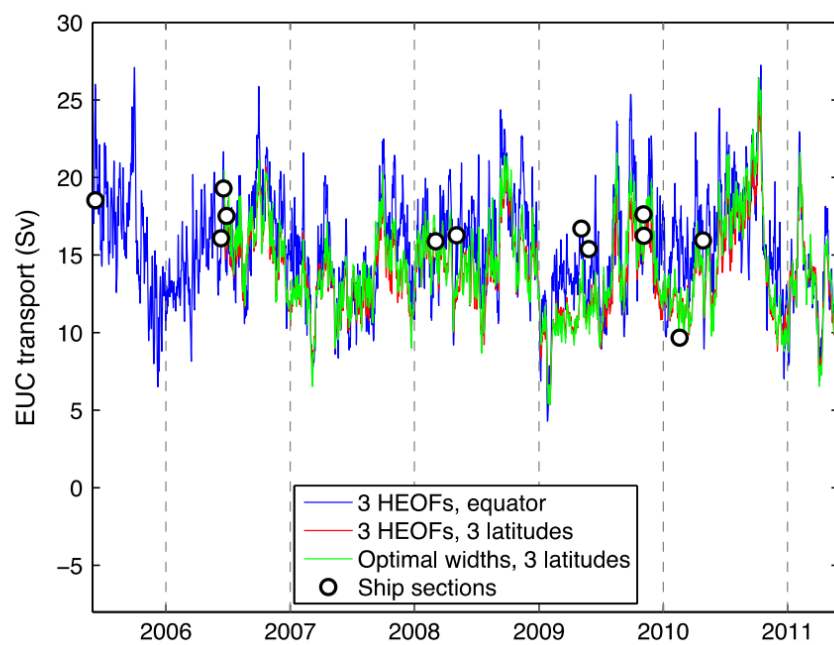


Figure 16: EUC tranports from Brandt et al. 2014 (their Fig. 5)

Next step:

- compare mean zonal currents of model and observation along 23°W
- [] update 23°W section for observations (work in progress)
- [] used the last 20 years for CORE (does not cover observational period).
- calculate transport (core position and depth) of zonal currents based on Hsin and Qiu (2012)
- [] EUC (advantage: mooring timeseries to reconstruct transport, Brandt et al. (2014))
- [] NEUC (advantage: mooring timeseries to reconstruct transport, Kristin Burmeister et al. (2020))
- [] SEUC
- [] (s/c/n)SEC
- [] NECC? (close to model boundary, velocity reverses in the western basin during seasonal cycle which can lead to artefacts in core position and tranport based on the algorithm of Hsin and Qiu (2012))
- Statistics to compare currents in observations and model:
 - [] Mean of current strength, meridional position, core depth
 - [] Standard deviation of current strength, meridional position, core depth
 - [] dominant frequencies of currents strength
 - [] long-term trend of current sterngh
 - [] Semiannual and annual cycle
- Connecton between wind field and currents:
 - [] linear regression of currents onto zonal wind field between 10°S and 10°N
 - [] Monthly or annual averaged data? Is monthly data enough?
- To indentify longterm variability in windforcing:
 - [] Calculate frequency spectra (Averaged in which boxes?)
 - [] Low-pass filter data at appropriate frequency (to focus on multidecadal variability)
 - [] Calculate HEOF of zonal wind field between 10°S and 10°N

Data and Methods

- INALT20 simulation forced by CORE v2 and JRA55-do
- Ship section along 23°W to validate model, maybe also sections along 5°S and 11°S (NBC), some section further west (35°W)
- Algorithm to estimate current core position and transport after Hsin and Qiu (2012)

Zonal current characterization

For both, INALT20 and the observational data we calculate the central position $\$ Y_{CM} \$$ and along-pathway intensity $\$ INT \$$ of the NEUC using the algorithm of Hsin and Qiu (2012).

$$Y_{CM}(x, t) = \frac{\int_{Z_l}^{Z_u} \int_{Y_S}^{Y_N} y u(x, y, z, t) dy dz}{\int_{Z_l}^{Z_u} \int_{Y_S}^{Y_N} u(x, y, z, t) dy dz} \quad (1)$$

$$INT(x, t) = \int_{Z_l}^{Z_u} \int_{Y_{CM}-W}^{Y_{CM}+W} u(x, y, z, t) dy dz \quad (2)$$

where y is latitude, x is longitude, u is zonal velocity, z is depth, t is time, Z_u (Z_l) is upper (lower) boundary of the flow, Y_N (Y_S) is northern (southern) limit of the flow, and W is the half mean width of the flow.

The advantage of this method is that the transport calculation follows the current core avoiding artifacts if the current is meridionally migrating.

References

- Brandt, Peter, H. W. Bange, Donata Banyte, Marcus Dengler, S.-H. Didwischus, Tim Fischer, Richard J Greatbatch, et al. 2015. "On the role of circulation and mixing in the ventilation of oxygen minimum zones with a focus on the eastern tropical North Atlantic." *Biogeosciences* 12 (2): 489–512. doi:10.5194/bg-12-489-2015.
- Brandt, Peter, Andreas Funk, Alexis Tantet, William E. Johns, and Jürgen Fischer. 2014. "The Equatorial Undercurrent in the central Atlantic and its relation to tropical Atlantic variability." *Climate Dynamics* 43 (11): 2985–97. doi:10.1007/s00382-014-2061-4.
- Burmeister, K., J. F. Lübbecke, P. Brandt, and O. Duteil. 2019. "Interannual Variability of the Atlantic North Equatorial Undercurrent and Its Impact on Oxygen." *Journal of Geophysical Research: Oceans* 124 (4): 2348–73. doi:10.1029/2018JC014760.
- Burmeister, Kristin, Joke F. Luebbecke, Peter Brandt, Martin Claus, and Johannes Hahn. 2020. "Fluctuations of the Atlantic North Equatorial Undercurrent and Associated Changes in Oxygen Transports." *Geophysical Research Letters* 47 (13). doi:10.1029/2020GL088350.
- Griffies, Stephen M., Arne Biastoch, Claus Böning, Frank Bryan, Gokhan Danabasoglu, Eric P. Chassignet, Matthew H. England, et al. 2009. "Coordinated Ocean-ice Reference Experiments (COREs)." *Ocean Modelling* 26 (1-2). Elsevier Ltd: 1–46. doi:10.1016/j.ocemod.2008.08.007.
- Hahn, Johannes, Peter Brandt, Sunke Schmidtko, and Gerd Krahmann. 2017. "Decadal oxygen change in the eastern tropical North Atlantic." *Ocean Science* 13 (4): 551–76. doi:10.5194/os-13-551-2017.
- Hazeleger, Wilco, and Sybren Drijfhout. 2006. "Subtropical cells and meridional overturning circulation pathways in the tropical Atlantic." *Journal of Geophysical*

Research: Oceans 111 (3): 1–13. doi:10.1029/2005JC002942.

Hsin, Yi Chia, and Bo Qiu. 2012. “Seasonal fluctuations of the surface North Equatorial Countercurrent (NECC) across the Pacific basin.” *Journal of Geophysical Research: Oceans* 117 (6): 1–17. doi:10.1029/2011JC007794.

Oschlies, Andreas, Peter Brandt, Lothar Stramma, and Sunke Schmidtko. 2018. “Drivers and mechanisms of ocean deoxygenation.” *Nature Geoscience* 11 (7). Springer US: 467–73. doi:10.1038/s41561-018-0152-2.

Schmidtko, Sunke, Lothar Stramma, and Martin Visbeck. 2017. “Decline in global oceanic oxygen content during the past five decades.” *Nature* 542 (7641). Nature Publishing Group: 335–39. doi:10.1038/nature21399.

Schott, Friedrich A., Julian P. McCreary Jr., and Gregory C. Johnson. 2004. “Shallow Overturning Circulations of the Tropical-Subtropical Oceans.” *Earth’s Climate* 147: 261–304.

Schwarzkopf, Franziska U., Arne Biastoch, Claus W. Böning, Jérôme Chanut, Jonathan V. Durgadoo, Klaus Getzlaff, Jan Harlaß, et al. 2019. “The IN-ALT family – a set of high-resolution nests for the Agulhas Current system within global NEMO ocean/sea-ice configurations.” *Geoscientific Model Development Discussions*, 1–44. doi:10.5194/gmd-2018-312.

Tsujino, Hiroyuki, Shogo Urakawa, Hideyuki Nakano, R. Justin Small, Who M. Kim, Stephen G. Yeager, Gokhan Danabasoglu, et al. 2018. “JRA-55 based surface dataset for driving ocean–sea-ice models (JRA55-do).” *Ocean Modelling* 130 (October): 79–139. doi:10.1016/j.ocemod.2018.07.002.